

AEROTHERMODYNAMIC PERFORMANCE COMPARISON OF ROUND AND FLAT-NOSE LEADING EDGES AT HYPERSONIC FLIGHT SPEED

Wilson F. N. Santos

National Institute for Space Research
Combustion and Propulsion Laboratory
12630-000 Cachoeira Paulista, SP, Brazil
wilson@lcp.inpe.br

Abstract. A numerical study is reported on a new family of blunt leading edges, flat-nose leading edges, situated in a rarefied hypersonic flow. The work is motivated by interest in investigating the aerothermodynamic characteristics of these new shapes as possible candidates for blunting geometry of hypersonic leading edges. The sensitivity of the stagnation point heating, total drag and shock wave standoff distance to nose-thickness and partial surface accommodation is calculated by using the Direct Simulation Monte Carlo (DSMC) method in combination with the Cercignani-Lampis-Lord gas surface interaction model. Comparisons based on equivalent stagnation point heating, equivalent total drag and equivalent shock standoff distance are made between flat-nose leading edges and round leading edges, usually assumed as the appropriate blunting geometry for heat transfer considerations. For the flow conditions considered, round leading edges provided lower drag and smaller shock standoff distance than the majority of the flat-nose leading edges for equivalent stagnation point heating. It was also found that flat-nose shapes yielded much smaller shock standoff distance than round leading edges for equivalent total drag. The analysis also showed that flat-nose shapes performed better than round leading edges for those cases with nose thickness of the order of the freestream mean free path.

Keywords: hypersonic flow, rarefied flow, DSMC, blunt leading edge, gas-surface interaction.

1. Introduction

In the past decade there has been a resurgence of interest in rarefied hypervelocity flows. This interest can be chiefly attributed to the fact that a greater understanding of rarefied hypervelocity flows is required to optimize the design of hypersonic configurations and re-entry vehicles. Hypersonic vehicles are generally characterized by slender bodies and sharp leading edges in order to achieve good aerodynamic properties like high lift and low drag. Nevertheless, at high Mach numbers, the vehicle leading edges should be sufficiently blunt in order to reduce the heat transfer rate to acceptable levels. The use of blunt-nose shapes tends to alleviate the aerodynamic heating problem since the heat flux for blunt bodies is far lower than that for sharply pointed bodies. Due mainly to manufacturing problems and the extremely high temperatures attained in hypersonic flight, hypersonic vehicles will have blunt nose, although probably slendering out at a short distance from the nose. Therefore, designing a hypersonic vehicle leading edge involves a tradeoff between making the leading edge sharp enough in order to obtain acceptable aerodynamic and propulsion efficiency and blunt enough to reduce the aerodynamic heating in the stagnation point.

Recently, considerable attention (Santos, 2003, 2004, 2005a, 2005b and 2005c) has been given to the problem of calculating aerodynamic characteristics of flat-nose leading edges at low-density hypersonic flight speed. The major interest in these works has gone into considering flat-nose shapes as possible candidates for blunting geometry of hypersonic leading edges, such as hypersonic waverider vehicles, which have been considered for high-altitude/low-density applications. Of particular significance on flat-nose shapes are the works by Santos (2005a, 2005b and 2005c). For the idealized situation of two-dimensional rarefied hypersonic flow, a parametric study has been performed on these shapes with a great deal of emphasis placed on the gas-surface interaction effects. Gas-surface interaction is the dominant physical process governing aerodynamic forces and heat transfer in hypersonic flight at high altitudes. The aerodynamic surface quantities and the state of the gas adjacent to the body surface are very sensitive to the assumptions used in the calculation concerning the gas-surface interaction model for transitional and free molecular flows. Therefore, the primary goal of those papers has been to assess the sensitivity of the flowfield structure (Santos, 2005a), aerodynamic surface quantities (Santos, 2005b) and shock wave structure (Santos, 2005c) to variations on the surface accommodation coefficients experienced by the leading edges.

In continuation of the aerothermodynamic investigation of flat-nose shapes under hypersonic transitional flow conditions, this work extends the analysis presented by Santos (2005a, 2005b and 2005c) by comparing flat-nose shapes with round leading edges with partial surface accommodation. The main idea is to provide information on how well these shapes stand up as possible candidates for blunting geometry of hypersonic leading edges. Comparison based on geometry, stagnation point heating, total drag and shock standoff distance are made to examine the benefits and disadvantages of using flat-nose shapes over round leading edges. Two method of comparison will be investigated: (1) flat-nose shapes are compared to a corresponding round leading edge, which generates the flat-nose shapes, and (2) flat-nose shapes are compared to an equivalent round leading edge, which is generated from the computational results for the flat-nose shapes. The equivalent round leading edge will yield the same stagnation point heating, the same drag coefficient or the same shock standoff distance as the computed solutions presented for flat-nose shapes. Thus, for the equivalent stagnation point heating, for instance, the total drag coefficient and the shock standoff distance will be the basis of comparison between these leading edges, and these properties will determine which geometry performs better.

2. Leading Edge Geometry Definition

The geometry of the leading edges considered in this work is the same as that presented in Santos (2003). The blunt shapes consist of a flat nose supplemented by an afterbody surface defined, in dimensionless form, by the following contour,

$$\bar{x} = \int_{\bar{y}=1}^{\bar{y}=\bar{y}_{\max}} \sqrt{\bar{y}^k - 1} d\bar{y} \quad \text{where } \bar{x} = x/y_{\text{nose}} \text{ and } \bar{y} = y/y_{\text{nose}} \quad (1)$$

The flat-nose shapes are modeled by assuming a sharp leading edge of half angle θ with a circular cylinder of radius R inscribed tangent to the wedge. The flat-nose shapes, inscribed between the wedge and the cylinder, are also tangent to them at the same common point where they have the same slope angle. It was assumed a leading edge half angle of 10 degree, a circular cylinder diameter of 10^{-2} m and flat-nose thickness t/λ_∞ of 0.01, 0.1 and 1, where $t = 2y_{\text{nose}}$ and λ_∞ is the freestream mean free path. From geometric considerations, the exponent k in Eq. (1) is obtained by matching slope on the wedge, circular cylinder and on the body shapes at the tangency point. For dimensionless thickness t/λ_∞ of 0.01, 0.1 and 1, the exponent k corresponds to 0.501, 0.746 and 1.465, respectively.

The round leading edges are modeled by following the same procedure adopted for the flat-nose leading edges. Figure 1(a) illustrates this construction for flat-nose leading edge with thickness t/λ_∞ of 1 and a round leading edge with a generic nose radius R_N .

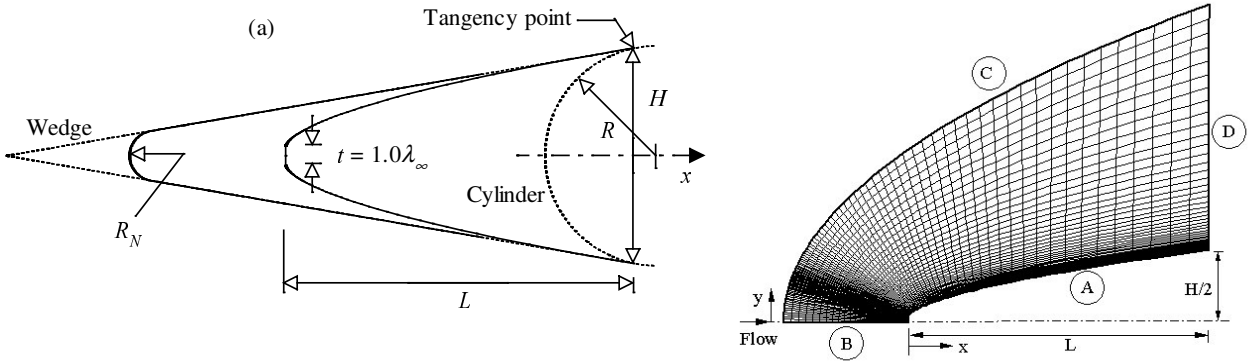


Figure 1: Drawing illustrating (a) the leading edge shapes and (b) the computational domain.

3. Computational Method and Procedure

The Direct Simulation Monte Carlo (DSMC) method introduced by Bird (1994) in the early 1960's has become the standard technique for simulating low-density gas dynamics. The DSMC method is based on tracking the movement of thousands to millions of representative molecules as they move through physical space while undergoing collisions among themselves as well as with any surface boundaries that may be present.

Collisions in the present DSMC code are modeled by using the variable hard sphere (VHS) molecular model (Bird, 1981) and the no time counter (NTC) collision sampling technique (Bird, 1989). Repartition energy among internal and translational modes is controlled by the Borgnakke-Larsen statistical model (Borgnakke and Larsen, 1975). Simulations are performed using a non-reacting gas model for a constant freestream gas composition consisting of 76.3% of N_2 and 23.7% of O_2 . Energy exchanges between the translational and internal modes, rotational and vibrational, are considered. Relaxation collision numbers of 5 and 50 were used for the calculations of rotation and vibration, respectively.

The computational domain used for the calculation is made large enough so that body disturbances do not reach the upstream and side boundaries, where freestream conditions are specified. A schematic view of the computational domain is depicted in Fig. 1(b). Side A is defined by the body surface. Reflection with incomplete surface accommodation is the condition applied to this side. Advantage of the flow symmetry is taken into account, and molecular simulation is applied to one-half of a full configuration. Thus, side B is a plane of symmetry. In such a boundary, all flow gradients normal to the plane are zero. At the molecular level, this plane is equivalent to a specular reflecting boundary. Side C is the freestream side through which simulated molecules enter and exit. Finally, the flow at the downstream outflow boundary, side D, is predominantly supersonic and vacuum condition is specified (Bird, 1994). At this boundary, simulated molecules can only exit.

DSMC simulations have been performed for an altitude of 70 km based on the flow conditions given by Santos (2003) and summarized in Tab. 1. The freestream velocity V_∞ , assumed to be constant at 3.56 km/s, corresponds to

freestream Mach number M_∞ of 12. The leading edge surface has a temperature T_w of 880 K for all cases considered. This temperature is chosen to be representative of the surface temperature near the stagnation point and is assumed to be uniform over the bodies.

Table 1: Freestream Conditions

Temperature T_∞ (K)	Pressure p_∞ (N/m ²)	Density ρ_∞ (kg/m ³)	Number density n_∞ (m ⁻³)	Viscosity μ_∞ (Ns/m ²)	Mean free path λ_∞ (m)	Velocity V_∞ (m/s)
220.0	5.582	8.753×10^{-5}	1.8209×10^{21}	1.455×10^{-5}	9.03×10^{-4}	3560

Based on the freestream conditions, the overall Knudsen number Kn_t , defined as the ratio of the freestream mean free path λ_∞ to the leading edge thickness t , corresponds to 1, 10 and 100 for leading edge thickness t/λ_∞ of 1, 0.1 and 0.01, respectively. The Reynolds number Re_t covers the range from 0.193 to 19.3, also based on conditions in the undisturbed stream with leading edge thickness t as the characteristic length.

The incomplete surface accommodation was simulated by the Cercignani-Lampis-Lord (CLL) model (Lord, 1991), which considers the normal α_n and tangential σ_t accommodation coefficients as the two adjustable parameters. The DSMC calculations were performed independently for three distinct numerical values for α_n and σ_t : 0.5, 0.75 and 1. It is important to mention that α_n and σ_t equal to 1 represent the diffusion reflection case.

4. Computational Results and Discussion

The purpose of this section is to discuss differences in the heat transfer, total drag and shock standoff distance due to variations on the leading edge thickness and on the surface accommodation coefficient, and to compare them to round shapes. Comparisons based on geometry are made to examine the benefits and disadvantages of using these blunt geometries over round shapes. In order to present the comparison coherently, it is necessary to repeat the results of previous publication to some extent. In doing so this section begins with part of the results for flat-nose shapes presented by Santos (2005b and 2005c).

5.1. Flat-Nose Shape

The heat flux q_w to the body surface is calculated by the net energy flux of the molecules impinging on the surface. The net heat flux q_w is related to the sum of the translational, rotational and vibrational energies of both incident and reflected molecules. A flux is regarded as positive if it is directed toward the surface. The heat flux q_w is normalized by the freestream kinetic energy flux $\frac{1}{2}\rho_\infty V_\infty^3$ and presented in terms of heat transfer coefficient C_h .

The heat transfer coefficient C_h for flat-nose leading edges is illustrated in Figs. 2(a-c) as a function of the dimensionless arc length S ($\equiv s/\lambda_\infty$) measured from the stagnation point. Figures 2(a-c) correspond to the diffuse reflection case, α_n of 0.5 and σ_t of 0.5, respectively. For comparison purpose, this set of figures also illustrates the heat transfer coefficient C_h for the reference round leading edge (circular cylinder).

It is apparent from Figs. 2(a-c) that C_h is sensitive to the leading edge thickness as well as to the normal and tangential accommodation coefficients. The heat transfer coefficient remains essentially constant over the first half of the front surface, but then increases in the vicinity of the flat-face/afterbody junction for the bluntest case investigated, $Kn_t = 1$ ($t/\lambda_\infty = 1$). Subsequently, C_h decreases sharply and continues to decline along the body surface.

It is also found that C_h decreases with decreasing α_n , not only for the flat-nose bodies but also for the circular cylinder. On the other hand, C_h increases with decreasing σ_t for the leading edges investigated. An understanding of this opposite behavior is gained by considering independently the contribution of the incident and reflected heat fluxes. Santos (2005b) showed that with the reduction on α_n , the number flux was slightly reduced. In addition to that, the buildup of particle density near the body surface was slightly reduced (Santos, 2005a), allowing the molecules oncoming from the freestream to transfer more energy to the body surface. Nevertheless, the reflected heat flux was almost identical as α_n changes from 1 to 0.5. As a result, the net heat flux to the body surface increased. In contrast, σ_t exhibits an opposite behavior on the heat transfer coefficient in that the incident heat transfer coefficient decreases and the reflected heat transfer coefficient increases as σ_t changes from 1 to 0.5. Consequently, a significant reduction is observed in the net heat flux to the body surface.

Usually, the stagnation region is generally considered as being one of the most thermally stressed zones in sharp/blunt bodies. Nevertheless, as a flat nose is introduced in these bodies, the most severe heat transfer region moves to the flat-face/afterbody junction with the nose thickness rise. The net heat flux depends on the number of molecules impinging on the body surface and on the velocity of the molecules. As shown by Santos (2005b), the number of molecules impinging on the front surface decreases in the vicinity of the flat-face/afterbody junction, then the velocity of the molecules increases as the flow approaches the junction of the leading edge in order to increase the heat transfer coefficient.

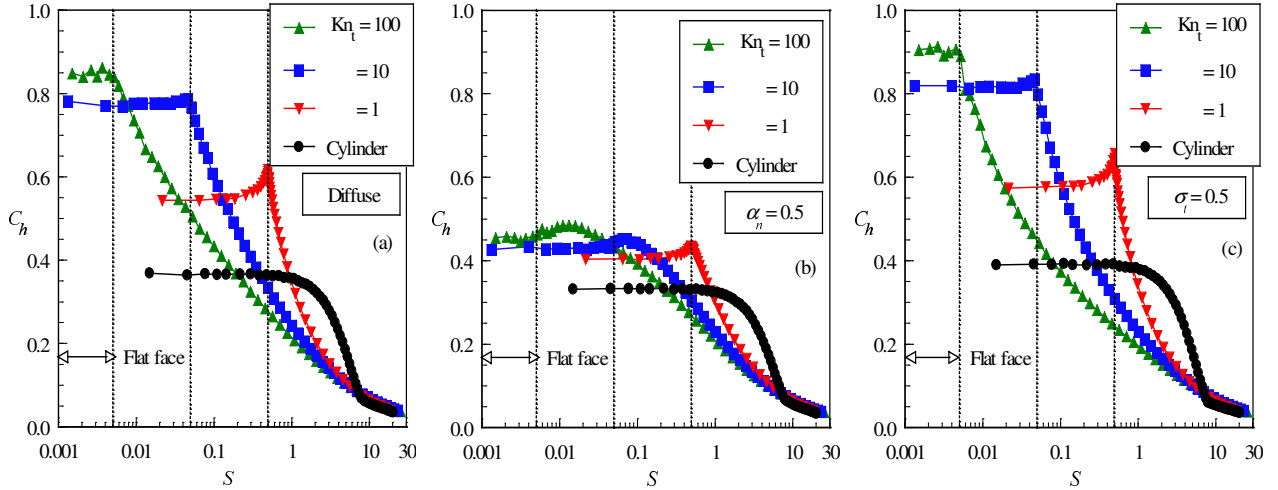


Figure 2: Comparison of heat transfer coefficient C_h along the body surface for flat-nose shapes and circular cylinder by considering (a) diffuse reflection, (b) α_n of 0.5 and (c) σ_t of 0.5.

In contrast to the flat-nose bodies, the heat transfer coefficient C_h for the circular cylinder remains essentially constant over the first half of the cylindrically portion of the leading edge, but then decreases sharply up to the cylinder/wedge junction. In addition, the heat transfer coefficient over the circular cylinder varies by an order of magnitude from the stagnation point to the cylinder/wedge junction. It is clearly seen from Figs. 2(a-c) that the general shape of the heat transfer coefficient C_h for the circular cylinder is preserved when normal or tangential accommodation coefficient is reduced from 1 to 0.5.

At this point, it seems important to compare the heat transfer coefficient at the stagnation point for the flat-nose shapes ($C_{ho})_{fn}$ with that for the circular cylinder ($C_{ho})_{cc}$ that generated the flat-nose shapes. Table 2 displays the heat transfer coefficient at the stagnation point for flat-nose shapes and the reference circular cylinder as a function of the surface accommodation coefficient. According to Tab. 2, a substantial reduction in the heat transfer coefficient at the stagnation point is obtained not only by increasing the frontal surface but also by reducing the normal accommodation coefficient. As a reference, for the diffuse case, ($C_{ho})_{fn}$ for Kn_t of 100, 10 and 1 is around 2.3, 2.1 and 1.5 times, respectively, of that for reference circular cylinder ($C_{ho})_{cc}$. In contrast, for the $\alpha_n = 0.5$ case, ($C_{ho})_{fn}$ for Kn_t of 100, 10 and 1 is around 1.4, 1.3 and 1.2 times, respectively, of that for the circular cylinder.

Table 2: Stagnation point heating comparison for flat-nose shapes and reference circular cylinder.

	$Kn_t = 100$	$Kn_t = 10$	$Kn_t = 1$	Cylinder
Diffuse	0.851	0.775	0.546	0.366
$\alpha_n = 0.75$ (0.50)	0.671 (0.454)	0.598 (0.429)	0.488 (0.404)	0.351 (0.333)
$\sigma_t = 0.75$ (0.50)	0.888 (0.904)	0.806 (0.817)	0.567 (0.578)	0.377 (0.391)

The drag on a surface in a gas flow results from the interchange of momentum between the surface and the molecules colliding with the surface. The total drag is obtained by the integration of the pressure p_w and shear stress τ_w distributions along the body surface, i.e., from the nose of the leading edge to the station L (see Fig. 1(b)), which corresponds to the tangent point common to all of the body shapes. The total drag presented in this section was obtained by assuming the shapes acting as leading edges. Consequently, no base pressure effects were taken into account on the calculations. The DSMC results for total drag are normalized by flux $\frac{1}{2}\rho_\infty V_\infty^2 H$ and presented as total drag coefficient C_d and its components of pressure drag C_{pd} and skin friction drag C_{fd} coefficients.

The impact of partial accommodation coefficient on the total drag coefficient C_d for the flat-nose shapes is demonstrated in Fig. 3 along with the total drag coefficient for the reference circular cylinder case. Figures 3(a-c) correspond to the diffuse reflection case, normal and tangential accommodation coefficients of 0.5, respectively. It is seen that as the leading edge becomes flatter the contribution of the pressure drag C_{pd} to the total drag C_d increases and the contribution of the skin friction drag C_{fd} decreases. For the Kn_t of 100 and 10, the major contribution to the total drag coefficient is attributed to the skin friction coefficient, a characteristic observed in sharp leading edges. In contrast, for the Kn_t of 1 as well as for the circular cylinder case, the major contribution to the total drag coefficient is attributed to the pressure, a blunt leading edge characteristic.

In what follows, the effect of changing independently the normal and tangential accommodation coefficients on the total drag coefficient C_d for the leading edge shapes is tabulated in Tab. 3. For comparison purpose, the total drag coefficient C_d obtained by Santos (2003) by considering diffuse reflection is also included in this table.

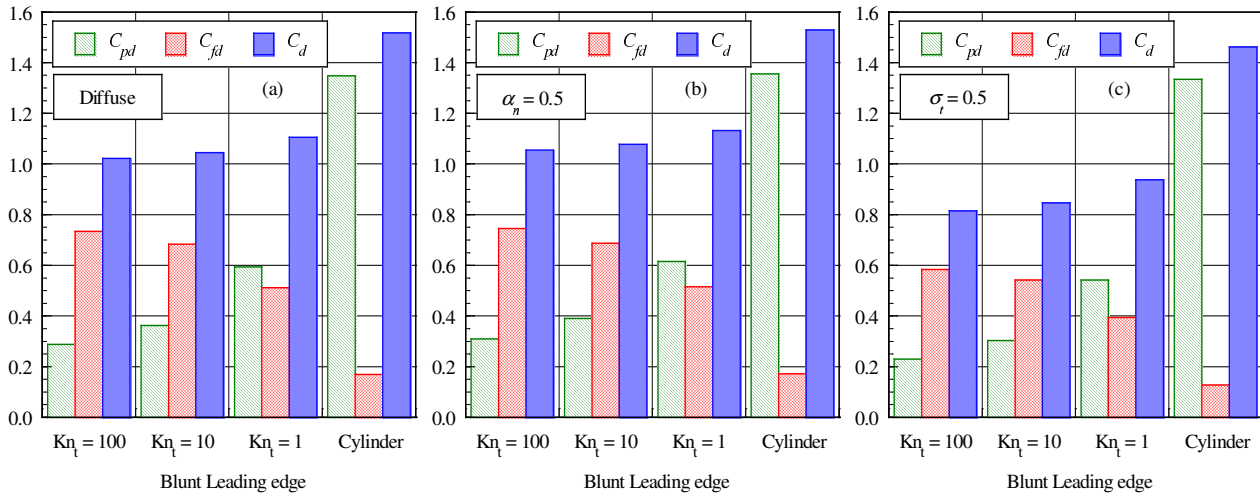


Figure 3: Comparison of pressure drag C_{pd} , skin friction drag C_{fd} and total drag coefficient C_d for flat-nose shapes and circular cylinder by considering (a) diffuse reflection, (b) α_n of 0.5 and (c) σ_t of 0.5.

Referring to Tab. 3, it can be seen that variations in α_n or σ_t have a different effect on the total drag coefficient. The total drag coefficient C_d increases around 2% or 3% by a reduction in the normal accommodation coefficient, and decreases by a reduction in the tangential accommodation coefficient for the leading edge shapes investigated. It is clearly seen that the tangential accommodation coefficient effect is more pronounced for the Kn_t of 100 and 10 than that for Kn_t of 1 and the circular cylinder. At this point, it should be emphasized that the flat-nose leading edges present distinct aerodynamic behavior in the sense that they are sharp for thickness $t/\lambda_\infty = 0.01$ and 0.1, and blunt for $t/\lambda_\infty = 1$ and for the reference circular cylinder.

The shock wave standoff distances for flat-nose shapes have been already calculated by Santos (2005b), where the procedure used in order to obtain them is described in details. Therefore, only the results will be presented in this work. Table 4 displays the shock wave standoff distance Δ , normalized by the freestream mean free path λ_∞ for the flat-nose leading edges investigated. According to Tab. 4, there is a discrete shock standoff distance for all cases investigated. Moreover, the shock standoff distance decreases with decreasing the nose thickness; as the leading edge becomes aerodynamically sharp. In addition, of great significance in this table is the impact of the partial surface accommodation on the leading edges. Except for the $Kn_t = 100$ case, the shock standoff distance increases by a reduction in the normal accommodation coefficient and decreases with decreasing the tangential accommodation coefficient. Compared to flat-nose shapes, the reference circular cylinder provides a larger shock detachment. As a reference, the circular cylinder presents a Δ/λ_∞ of 1.645 for the diffuse case. This value is about 8.2, 4.8 and 2.2 times larger than that for the Kn_t of 100, 10 and 1, respectively.

Table 3: Total drag coefficient comparison for flat-nose shapes and the reference circular cylinder.

	$Kn_t = 100$	$Kn_t = 10$	$Kn_t = 1$	Cylinder
Diffuse	1.022	1.046	1.106	1.518
$\alpha_n = 0.75$ (0.50)	1.038 (1.055)	1.060 (1.078)	1.118 (1.132)	1.523 (1.528)
$\sigma_t = 0.75$ (0.50)	0.957 (0.815)	0.982 (0.846)	1.048 (0.937)	1.496 (1.462)

Table 4: Dimensionless shock standoff distance comparison for flat-nose shapes and the reference circular cylinder.

	$Kn_t = 100$	$Kn_t = 10$	$Kn_t = 1$	Cylinder
Diffuse	0.201	0.345	0.753	1.645
$\alpha_n = 0.75$ (0.50)	0.157 (0.151)	0.421 (0.459)	0.867 (1.008)	1.728 (1.805)
$\sigma_t = 0.75$ (0.50)	0.107 (0.049)	0.265 (0.212)	0.696 (0.656)	1.620 (1.541)

The displacement of the shock wave is especially undesirable in waverider geometry, because this hypersonic configuration usually depends on shock wave attachment at the leading edge to achieve its high lift-to-drag ratio at high-lift coefficient. Shock wave detachment will allow pressure leakage from the lower surface of the vehicle to the upper surface, thereby degrading the aerodynamic performance of the vehicle. In this context, the flat-nose leading edges seem to be more appropriate than the reference circular cylinder, since they present reduced shock wave detachment distances as compared to the circular cylinder.

5.2. Round Leading Edges

In order to compare flat-nose leading edge with round leading edge, it becomes imperative to determine the dependence of heat transfer, total drag and shock standoff distance on the nose radius for round leading edge. In this connection, Santos (2005d) has investigated these properties for a family of round leading edges. DSMC simulations were performed for four round leading edges, besides the reference round leading edge (circular cylinder), with nose radii R_N/λ_∞ of 0.02, 0.1, 1.0, and 2.0, which correspond to overall Knudsen number Kn_D of 25, 5, 0.5 and 0.25, respectively, by assuming the nose diameter as the characteristic length.

Distributions of the heat transfer coefficient C_h along the round leading edge surface are illustrated in Fig. 4 with the dimensionless nose radius R_N/λ_∞ as a parameter. Figures 4(a-c) correspond to the diffuse reflection case, normal and tangential accommodation coefficients of 0.5, respectively. It is observed from this set of figures that altering not only the nose radius but also the accommodation coefficient produces a substantial change in the heat transfer coefficient in the cylindrically blunt portion of the leading edge. In general, the heat transfer coefficient presents the maximum value at the stagnation point and drops off sharply along the cylindrically blunt portion up to the cylinder/wedge junction. Also, the heat transfer coefficient at the stagnation region decreases with increasing the nose radius. This behavior seems to be in agreement with the continuum predictions for blunt body in that the heat flux scales inversely with the square root of the nose radius. The heat transfer coefficient at the stagnation point C_{ho} is displayed in Tab. 5 for the nose radii investigated. These values were obtained by a curve fitting process performed over the curves displayed in Fig. 4.

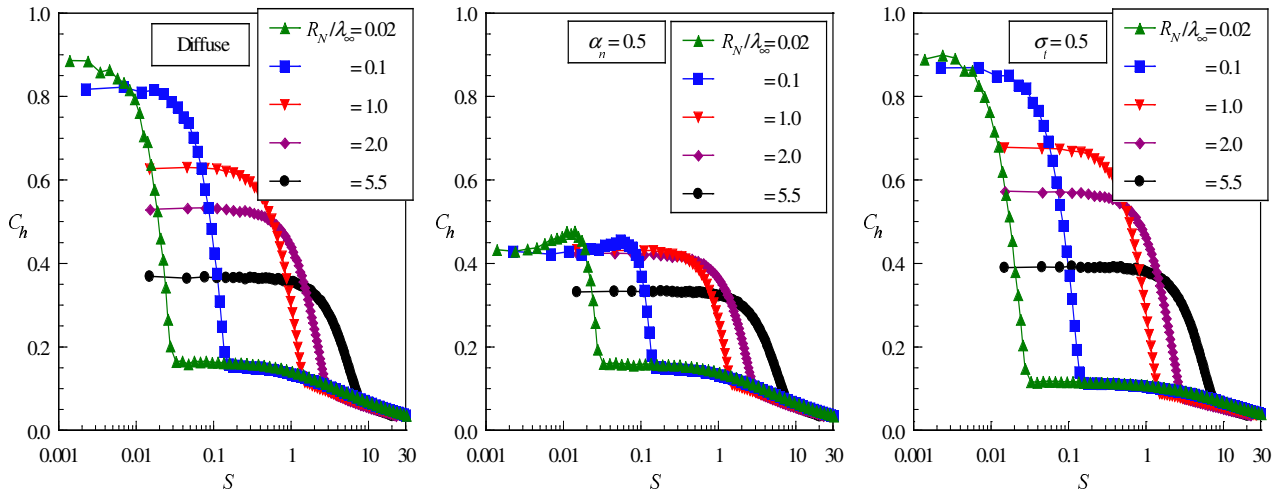


Figure 4: Heat transfer coefficient C_h along the body surface for round leading edges as a function of the nose radius by considering (a) diffuse reflection, (b) α_n of 0.5 and (c) σ_t of 0.5.

The dependence of the total drag coefficient C_d on the nose radius is shown in Tab. 6. It is apparent from this table that the total drag coefficient increases with increasing the nose radius. In general, the contributions of the pressure drag C_{pd} to the total drag increases with the nose radius and the contribution of the skin friction drag C_{fd} diminishes with the nose radius rise. In addition, the total drag coefficient is affected by a reduction on either normal or tangential accommodation coefficient, as would be expected.

Table 5: Heat transfer coefficient at the stagnation point C_{ho} for round leading edges.

R_N/λ_∞	0.02	0.1	1	2	5.5
Diffuse	0.883	0.824	0.630	0.532	0.366
$\alpha_n = 0.75$ (0.50)	0.660 (0.436)	0.622 (0.433)	0.537 (0.429)	0.484 (0.424)	0.352 (0.333)
$\sigma_t = 0.75$ (0.50)	0.894 (0.904)	0.859 (0.868)	0.660 (0.676)	0.553 (0.571)	0.377 (0.391)

Table 6: Total Drag coefficient C_d for round leading edges.

R_N/λ_∞	0.02	0.1	1	2	5.5
Diffuse	0.978	0.979	1.028	1.085	1.519
$\alpha_n = 0.75$ (0.50)	0.994 (1.011)	0.995 (1.012)	1.039 (1.057)	1.144 (1.158)	1.523 (1.528)
$\sigma_t = 0.75$ (0.50)	0.908 (0.766)	0.910 (0.767)	0.957 (0.837)	1.074 (0.975)	1.496 (1.462)

The dimensionless shock wave standoff distance Δ/λ_∞ for round leading edges is tabulated in Tab. 7. According to Tab. 7, there is a discrete shock standoff distance for the round leading edge cases investigated. Furthermore, the shock standoff distance decreases with diminishing the nose radius. This is an expected result since shock standoff distance on a circular cylinder scales with the nose radius. Similar to the total drag coefficient, the shock standoff distance is also affected by changes on normal and tangential accommodation coefficients.

Table 7: Dimensionless shock wave standoff distance Δ/λ_∞ for round leading edges.

R_N/λ_∞	0.02	0.1	1	2	5.5
Diffuse	0.114	0.226	0.598	0.845	1.646
$\alpha_n = 0.75$ (0.50)	0.104 (0.096)	0.260 (0.249)	0.727 (0.858)	0.956 (1.075)	1.728 (1.805)
$\sigma_t = 0.75$ (0.50)	0.074 (0.058)	0.159 (0.117)	0.551 (0.504)	0.818 (0.757)	1.620 (1.541)

5.3. Equivalent Round Leading Edges

The stagnation point heating, the total drag and the shock wave standoff distance for flat-nose leading edges have been compared to those for the reference round leading edge (circular cylinder) in the previous sections. A second means of comparison between flat-nose shapes and round leading edges is defined as equivalent round leading edge. Equivalent round leading edge, or equivalent nose radius, is found by assuming the same value for the stagnation point heating, total drag or shock standoff distance provided by the flat-nose leading edges. For instance, by holding the stagnation point heating the same, the total drag and the shock standoff distance for the equivalent round leading edge may be compared to those for flat-nose leading edges in order to determine which shape is better suited for leading-edge blunting. A similar procedure is repeated for the total drag and for the shock standoff distance.

A summary of the computed data for the heat transfer coefficient at the stagnation point C_{ho} , the total drag coefficient C_d and the shock standoff distance Δ/λ_∞ for round leading edge is displayed in Fig. 5. In what follows, the stagnation point heating C_{ho} for flat-nose shapes displayed in Tab. 2 is used as an input in Fig. 5 in order to determine the equivalent nose radius $R_{N,eqv}$. With the equivalent nose radius, the total drag and the shock standoff distance that correspond to that equivalent nose radius are also obtained from Fig. 5 itself.

The comparison of the total drag coefficient and the shock standoff distance for flat-nose shapes, defined by Kn_t of 10 and 1, and for round leading edges with equivalent nose radii that match flat-nose body stagnation point heating is shown in Tab. 8. In this table, the numbers in the parenthesis correspond to $Kn_t = 1$ case. It is seen from this table that equivalent round leading edges with the same stagnation point heating than that for the $Kn_t = 10$, have slightly lower drag and smaller shock standoff distance than flat-nose bodies for the majority of the cases investigated. In contrast, flat-nose bodies perform better for the $Kn_t = 1$ case. As a reference, the case $Kn_t = 1$ and $\alpha_n = 0.5$, which is tangent to a 20-degree wedge (see Fig. 1(a)), has the same stagnation point heating as a round leading edge that is around 1.9 times smaller than the reference round leading edge that is also tangent to the wedge at the same point. Furthermore, this equivalent round leading edge has a total drag and a shock standoff distance that is 9.6% and 22.9%, respectively, larger than the corresponding flat-nose body. As a result, based on Tab. 8, for the same stagnation point heating, flat-nose bodies perform better than round leading edges for those cases with nose thickness $t/\lambda_\infty = 1$.

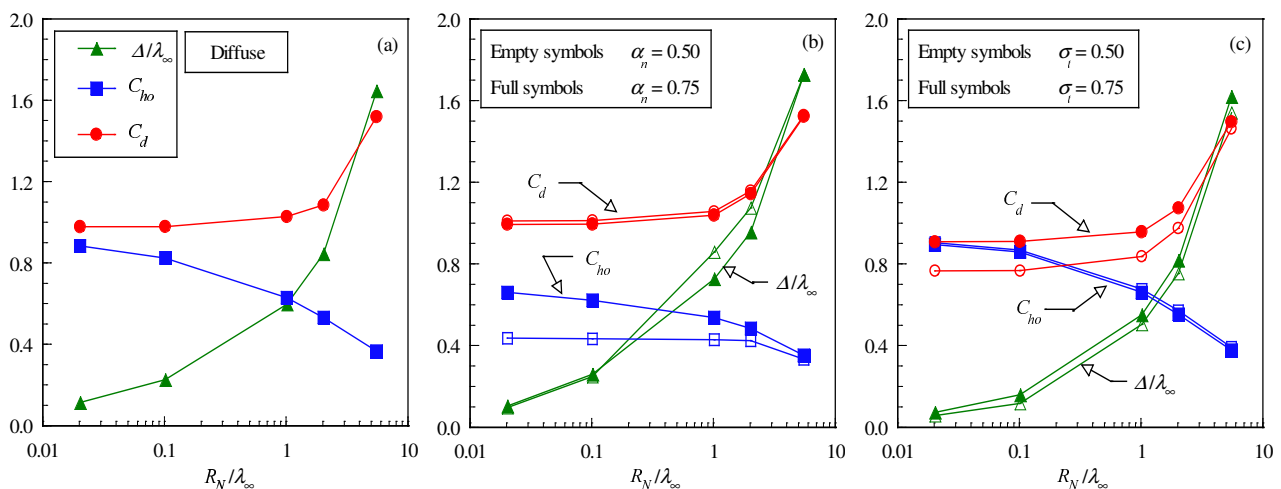


Figure 5: Heat transfer coefficient C_{ho} , total drag C_d and shock standoff distance Δ/λ_∞ for round leading edges as a function of the nose radius for (a) diffuse case, (b) normal α_n and (c) tangential σ_t accommodation coefficients.

By using the total drag coefficient C_d found previously for flat-nose leading edges, Tab. 3, an equivalent nose radius $R_{N,eqv}$ may be found from Fig. 5 that gives the same total drag coefficient as the flat-nose bodies. At this time, the stagnation point heating and the shock standoff distance will be the two important factors in order to determine which shape is better suited for leading edge blunting.

The comparison of the stagnation point heating and the shock standoff distance for flat-nose shapes and for round leading edges with equivalent nose radii that match flat-nose body total drag is tabulated in Tab. 9. It is clear from this table that equivalent round leading edges provide lower stagnation point heating than the flat-nose bodies defined by Kn_t of 10. Nonetheless, the equivalent round leading edges have much larger shock standoff distances than flat-nose shapes defined by Kn_t of 10. It is also apparent that, for flat nose shapes defined by Kn_t of 1, equivalent round leading edges provide larger stagnation point heating and shock standoff distance than flat-nose bodies. By taking the case $Kn_t = 10$ and $\alpha_n = 0.5$ as a reference, this shape has the same total drag as a round leading edge that is around 5.1 times smaller than the reference round leading edge (circular cylinder). Moreover, this equivalent round leading edge has a stagnation point heating that is around 20% smaller than the corresponding flat-nose body. In contrast, this equivalent round leading edge has a shock standoff distance that is 145% larger than that for the case $Kn_t = 10$ and $\alpha_n = 0.5$. As a matter of fact, larger displacement of the shock wave is an undesirable property for hypersonic waverider design, as mentioned earlier. Consequently, based on Tab. 10, round leading edges perform worse than flat-nose bodies as the shock standoff distance consideration is involved.

Another interesting result may be found from the shock standoff distance. The equivalent nose radius $R_{N,eqv}$ that yields the same shock standoff distance Δ/λ_∞ for each one of the flat-nose shapes shown in Tab. 4 may be determined from Fig. 5. The comparison of the stagnation point heating and the total drag coefficient for flat-nose shapes and for round leading edges with equivalent nose radius that matches flat-nose body shock standoff distance is tabulated in Tab. 10. It is observed from Tab. 10 that equivalent round leading edges provide smaller total drag and larger stagnation point heating than flat-nose shapes for the cases investigated.

Finally, a critical assessment of the results provided by Tabs. 8, 9 and 10 confirms the expected behavior for sharp and blunt leading edges. As the leading edge shape approaches the wedge shape (see Fig. 1(a)), the total drag decreases, the shock standoff distance decreases and the stagnation point heating increases. In contrast, as the leading edge shape approaches the circular cylinder, the total drag increases, the shock standoff distance increases and the stagnation point heating decreases. Thus, the ideal leading edge shape for hypersonic vehicle will depend on the context.

Table 8: Nose radius necessary for comparable stagnation point heating to flat-nose shapes.

Kn_t	α_n	σ_t	$R_{N,eqv}/\lambda_\infty$	$R/R_{N,eqv}$	$C_{d,eqv}/C_{d,fn}$	Δ_{eqv}/Δ_{fn}
10 (1)	1	1	0.334 (1.869)	16.599 (2.962)	0.948 (0.973)	0.912 (1.097)
10 (1)	0.75	1	0.359 (1.959)	15.433 (2.827)	0.951 (1.016)	0.930 (1.084)
10 (1)	0.50	1	0.956 (2.815)	5.794 (1.967)	0.977 (1.096)	1.783 (1.229)
10 (1)	1	0.75	0.344 (1.895)	16.106 (2.922)	0.939 (1.009)	0.992 (1.123)
10 (1)	1	0.50	0.343 (1.960)	16.122 (2.825)	0.928 (1.030)	1.033 (1.127)

Table 9: Nose radius necessary for comparable total drag coefficient to flat-nose shapes.

Kn_t	α_n	σ_t	$R_{N,eqv}/\lambda_\infty$	$R/R_{N,eqv}$	$C_{ho,eqv}/C_{ho,fn}$	Δ_{eqv}/Δ_{fn}
10 (1)	1	1	1.334 (2.198)	4.151 (2.519)	0.773 (0.957)	1.923 (1.203)
10 (1)	0.75	1	1.220 (1.781)	4.538 (3.109)	0.880 (1.019)	1.837 (1.038)
10 (1)	0.50	1	1.229 (1.768)	4.504 (3.132)	0.997 (1.054)	1.969 (1.011)
10 (1)	1	0.75	1.235 (1.809)	4.482 (3.061)	0.790 (1.016)	2.297 (1.091)
10 (1)	1	0.50	1.083 (1.752)	5.110 (3.160)	0.819 (1.037)	2.455 (1.048)

Table 10: Nose radius necessary for comparable shock standoff distance to flat-nose shapes.

Kn_t	α_n	σ_t	$R_{N,eqv}/\lambda_\infty$	$R/R_{N,eqv}$	$C_{ho,eqv}/C_{ho,fn}$	$C_{d,eqv}/C_{d,fn}$
10 (1)	1	1	0.410 (1.576)	13.509 (3.513)	0.979 (1.052)	0.952 (0.958)
10 (1)	0.75	1	0.416 (1.636)	13.295 (3.385)	0.991 (1.034)	0.953 (0.987)
10 (1)	0.50	1	0.417 (1.716)	13.284 (3.227)	1.005 (1.054)	0.953 (0.995)
10 (1)	1	0.75	0.348 (1.567)	15.881 (3.533)	0.999 (1.061)	0.939 (0.973)
10 (1)	1	0.50	0.327 (1.626)	16.946 (3.405)	1.004 (1.060)	0.927 (0.982)

6. Concluding Remarks

The computations of a rarefied hypersonic flow on blunt bodies have been performed by using the Direct Simulation Monte Carlo method. The calculations provided information concerning the nature of the stagnation point heating, the total drag and the shock standoff distance for a family of contours composed by a flat nose supplemented by a curved afterbody surface.

The aerothermodynamic performance of these blunt shapes was compared to a corresponding circular cylinder, typically used in blunting sharp leading edges for heat transfer considerations. It was found that the total drag is lower and the shock standoff distance is much smaller on the new blunt shapes than on the representative circular cylinder solution in this geometric comparison. Nevertheless, stagnation point heating for these flat-nose shapes is still higher than that for the corresponding circular cylinder. These flat-nose shapes behave as if they had a sharper profile than their representative circular cylinder. However, these shapes have more volume than the circular cylinder geometry. Hence, although stagnation point heating on these new shapes may be higher as compared to the circular cylinder, the overall heat transfer to these leading edges may be tolerate if there is active cooling because additional coolant may be placed in the leading edge. Moreover, the shock standoff distance on a cylinder scales with the radius of curvature, therefore cylindrical bluntness added for heating rate reduction will also tend to displace the shock wave, allowing pressure leakage. In this context, as the new shapes behave as if they were sharper profiles than the circular cylinder, then they present a better performance since they display smaller shock detachment distances than the corresponding circular cylinder.

In addition, equivalent round leading edges were defined with the same stagnation point heating, total drag or shock standoff distance yielded by the flat-nose shapes. With the same stagnation point heating as the flat-nose shapes, round leading edges were shown to produce slightly smaller total drag and smaller shock standoff distance for the majority of the cases investigated. The analysis also showed that, for the same total drag, round leading edges gave larger shock standoff distance than flat-nose shapes. For the equivalent shock standoff distance, the shapes exhibited approximately the same performance.

It is apparent that each comparison resulted in a different conclusion for which geometry perform better. Thus, the ideal blunting leading edge relies on the context. If shock standoff distance is the primary issue in leading edge design of hypersonic waveriders, then flat-nose leading edges are superior to round leading edges.

7. References

- Bird, G. A., 1981, "Monte Carlo Simulation in an Engineering Context", *Progress in Astronautics and Aeronautics: Rarefied gas Dynamics*, Ed. Sam S. Fisher, Vol. 74, part I, AIAA New York, pp. 239-255.
- Bird, G. A., 1989, "Perception of Numerical Method in Rarefied Gasdynamics", *Rarefied gas Dynamics: Theoretical and Computational Techniques*, Eds. E. P. Muntz, and D. P. Weaver and D. H. Capbell, Vol. 118, *Progress in Astronautics and Aeronautics*, AIAA, New York, pp. 374-395.
- Bird, G. A., 1994, "Molecular Gas Dynamics and the Direct Simulation of Gas Flows", Oxford University Press, Oxford, England, UK.
- Borgnakke, C. and Larsen, P. S., 1975, "Statistical Collision Model for Monte Carlo Simulation of Polyatomic Gas Mixture", *Journal of computational Physics*, Vol. 18, No. 4, pp. 405-420.
- Lord, R. G., 1991, "Application of the Cercignani-Lampis Scattering Kernel to Direct Simulation Monte Carlo Method", *Proceedings of the 17th International Symposium on Rarefied Gas Dynamics*, edited by A. E. Beylich, Aachen, Germany, pp. 1427-1433, July 8-14.
- Santos, W. F. N., 2003, "Aerodynamic Heating on Blunt Nose Shapes in Rarefied Hypersonic Flow", *Proceedings of the 17th International Congress of Mechanical Engineering, COBEM 2003*, 10-14 Nov, São Paulo, SP, Brazil.
- Santos, W. F. N., 2004, "Numerical Prediction of Stagnation-Point Shock-Detachment Distance for Hypersonic Low-Density Flow over Blunt Nose Shapes", *Proceedings of the 24th International Congress of the Aeronautical Sciences, ICAS 2004*, 29 Aug – 3 Sept, Yokohama, Japan.
- Santos, W. F. N., 2005a, "Gas-Surface Interaction Impact on Flowfield Structure of Low-Density Hypersonic Flow over Flat-Nose Bodies", *Proceedings of the 18th International Congress of Mechanical Engineering, COBEM 2005*, 6-11 Nov, Ouro Preto, MG, Brazil.
- Santos, W. F. N., 2005b, "Gas-Surface Interaction Impact on Aerodynamic Surface Quantities of Low-Density Hypersonic Flow over Flat-Nose Bodies", *Proceedings of the 18th International Congress of Mechanical Engineering, COBEM 2005*, 6-11 Nov, Ouro Preto, MG, Brazil.
- Santos, W. F. N., 2005c, "Gas-Surface Interaction Impact on Shock Wave Structure of Low-Density Hypersonic Flow over Flat-Nose Bodies", *Proceedings of the 18th International Congress of Mechanical Engineering, COBEM 2005*, 6-11 Nov, Ouro Preto, MG, Brazil.
- Santos, W. F. N., 2005d, "Simulation of Round Leading Edge Aerothermodynamics", *Proceedings of the 18th International Congress of Mechanical Engineering, COBEM 2005*, 6-11 Nov, Ouro Preto, MG, Brazil.